ARTICLE

Hydrate of neutral iron(III) complex based on pyruvic acid thiosemicarbazone ligand with abrupt spin-crossover with $T_{1/2}$=340 K and wide hysteresis loop of 45 K

Received 00th January 20xx,
Accepted 00th January 20xx

DOI: 10.1039/x0xx00000x

Maxim A. Blagov,[a] Alexander V. Akimov,[a] Anatoly S. Lobach,[a] Leokadiya V. Zorina,[b] Sergey V. Simonov,[b] Konstantin V. Zakharov[c], Alexander N. Vasiliev[c] and Nataliya G. Spitsyna*[a]

The hydrate of neutral iron(III) complex based on pyruvic acid thiosemicarbazone ligand [Fe^{III}(Hthpy)(thpy)]·H_2O (**1**) was synthesized and characterized using FT-IR spectroscopy, powder and single-crystal X-ray diffraction, *dc* magnetic measurements, EPR and ^{57}Fe Mössbauer spectroscopy. The crystal structure of **1** was determined for the first time. Two distinct chelating ligands $Hthpy^-$ and $thpy^{2-}$ coordinate the Fe(III) ion to form the $FeN_2O_2S_2$ octahedron which shows a low spin geometry at 150-350 K. The crystal packing contains infinite chains of the Fe(III) complexes as well as water molecules located in cavities. Along the chain, π-π interacting pairs of the Fe complexes are linked by H-bonding. According to the *dc* magnetic measurements, the complete abrupt spin-crossover with half-transition temperature-$T_{1/2}$=340 K and a hysteresis loop of 45 K occurs in the temperature range of 300–363 K. Based on the X-ray structure of **1**, the Bleaney–Bowers equation for the isolated dimer model was used to approximate the temperature dependence of the magnetic susceptibility in the range of 2–50 K. The defined intradimer exchange constant J_{exp}= −0.498(1) K corresponds to a weak antiferromagnetic exchange between the iron(III) magnetic centers. DFT calculations of H- and π-π bonded fragments of the crystal structure of **1** in the HS and LS states were carried out. Moreover, BS-DFT calculations confirm the presence of antiferromagnetic exchange J_{calc} = – 0.92 K in the π-π bonded pairs of the ferric complexes, and show the exchange pathway between Fe(III) ions by the calculated spin density distribution.

Introduction

Nowadays spin switching or spin-crossover (SCO) represents one of the most interesting phenomena in coordination chemistry of transition metals with d^4-d^7 electronic configuration.[1,2] The electronic transition of magnetic center between low-spin (LS) and high-spin (HS) states can be realized only at a suitable ligand field.[3] The tuning of a suitable energy gap between these spin states is realized by selecting an appropriate ligand defining the first coordination sphere of the metal ion.[4-5] Ligands can form cationic, neutral and anionic complexes upon chemical interaction with a transition metal cation.[6] Neutral complexes, unlike cationic or anionic complexes, do not have additional elements represented by outer-sphere counterions in the crystal lattice.[7-9] This reduces the number of factors that directly affect the parameters of spin-crossover, such as the shape of the temperature dependence curves of the magnetic susceptibility, the half-transition temperature ($T_{1/2}$) and the presence of hysteresis loop.[2,10] The compounds exhibiting an abrupt SCO with a wide hysteresis loop near room temperatures are considered to be the most suitable for further practical application as the components of modern electron devices.[11-13] In turn, neutral complexes can be formed by both homo- and heteroleptic ligands. The most common metal coordination complexes are those that contain two ligands of different nature, which allows for tuning of the supramolecular packing by controlling π-π and hydrogen interactions.[14-19] In this context the transition metal complexes with thiosemicarbazones formed by the corresponding organic substrates are unique, since these ligands (L) can coordinate to the metal ion in the mono- (HL^-) and di-anionic states (L^{2-}) (Fig. 1) due to the possibility of acidic proton loss and thione/thiol tautomerism.[17, 20] The affinity of thiosemicarbazone ligands for Fe(III) ions facilitates the formation of chemically stable SCO complexes, which also exhibit biological activity and antitumor properties. These complexes have attracted much attention from researchers since the first works by Zelentsov et al. published in the 1970s.[17]

Neutral thiosemicarbazone SCO complexes of Fe(III) can be formed by coordinating two chemical nonequivalent ligands, one in the monoanionic (thione) form and the other in the dianionic (thiol) form.[21-24] Pyruvic acid (py) thiosemicarbazones

[a] *Federal Research Center of Problems of Chemical Physics and Medicinal Chemistry, Russian Academy of Sciences, Chernogolovka, Moscow region 142432, Russia. E-mail: spitsina@icp.ac.ru*
[b] *Osipyan Institute of Solid State Physics, Russian Academy of Sciences, Chernogolovka, Moscow region 142432, Russia.*
[c] *Lomonosov Moscow State University, Moscow 119991, Russia.*

Supplementary Information available (ESI): Instrumental techniques; photo of the crystal (Fig. S1); XRPD (Fig. S2); thermogram (Fig. S3); ATR FT-IR absorption spectra for the H_2-thpy·⅓(H_2O) ligand and **1** (Fig. S4, Tab. S1-S2); details of X-ray analysis (Tab. S3-S7); *dc* magnetic (Fig. S5-S7), ^{57}Fe Mössbauer (Fig. S8, Tab. S8-S9) and DFT (Tab. S10-S22) data. CCDC 2389231 (150 K) and 2389232 (350 K). See DOI: https://doi.org/ 10.1039/x0xx00000x

(th) are known as ligands, that form neutral ferric complexes with the formula [Fe^{III}(Hthpy)(thpy)].

At the same time, Hendrickson et al. in 1985 investigated two forms of the neutral complex [Fe^{III}(Hthpy)(thpy)] and [Fe^{III}(Hthpy)(thpy)]·H_2O. The authors were unable to obtain single crystals suitable for X-ray diffraction analysis of both complexes due to their general insolubility, as well as their tendency to decompose in water.[21] Thus, it was concluded that the crystal packing of these complexes was similar to the established structure of [Cr^{III}(Hthpy)(thpy)]·H_2O. A hysteretic spin-transition with $T_{1/2}$=225 K and hysteresis loop of ΔT=10 K was established only for [Fe^{III}(Hthpy)(thpy)], whereas for [Fe^{III}(Hthpy)(thpy)]·H_2O was reported to be low-spin up to 300 K.[21, 24]

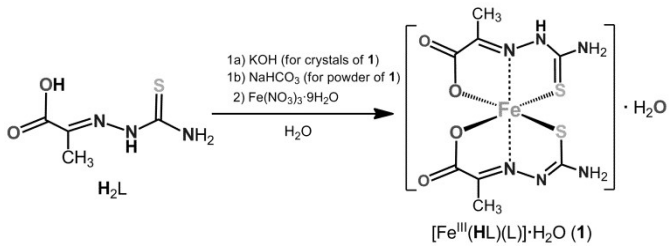

Fig. 1 Scheme of the synthesis of [Fe^{III}(Hthpy)(thpy)]·H_2O (**1**) complex.

In this work, we synthesized crystals and a single-phase sample of the neutral complex [Fe^{III}(Hthpy)(thpy)] H_2O (**1**) (Fig. 1, S1, 2†) and established its crustal structure for the first time. The crystal structure of **1** at 150 and 350 K contains π-π bonded pairs of this complex in the LS state, linked to each other by hydrogen bonds, which is directly confirmed by the proposed model for approximation of the temperature dependence of magnetic susceptibility in the range of 2–50 K. According to *dc* magnetic measurements, the complete abrupt SCO with $T_{1/2}$=340 K and a hysteresis loop of ΔT=45 K occurs in the temperature range of 300–363 K. The presence of a wide hysteresis loop was also confirmed by the data of high-temperature EPR and ^{57}Fe Mössbauer spectroscopy measurements. DFT calculations were carried out for the H- and π-π bonded pairs of crystal structure **1** in the HS and LS states.

Experimental section

Materials and methods

Thiosemicarbazide ($H_2NC(S)NHNH_2$), pyruvic acid ($CH_3COCOOH$), potassium hydroxide (KOH), sodium bicarbonate ($NaHCO_3$), and iron(III) nitrate nonahydrate ($Fe(NO_3)_3·9H_2O$) were obtained from Sigma-Aldrich. All chemicals were used without further purification.

Synthetic procedures

Synthesis of ligand H_2thpy·⅓H_2O. The synthesis of the free tridentate Schiff-base pyruvic acid thiosemicarbazone ligand (H_2thpy) was performed according to the literature experimental procedure.[25]

Synthesis of [Fe^{III}(Hthpy)(thpy)]·H_2O crystals (1). To a suspension of the H_2thpy·⅓H_2O ligand (0.5 g, 3 mmol) in 15 ml of water was added KOH (0.347 g, 6.2 mmol) in 10 ml of water with stirring at room temperature. After that, the resulting solution color turned pale yellow. Then a solution of $Fe(NO_3)_3·9H_2O$ (0.626 g, 1.5 mmol) in 7 ml of water was added dropwise with stirring. The mixture was stirred for 2 hours and left to evaporate under ambient conditions. Several black prism crystals of **1** (photo in Fig. S1†) suitable for single-crystal X-ray structural analysis were obtained after one week. The electron-probe X-ray microanalysis (EPMA) of *crystals* **1** afforded the elements in the ratio Fe:S = 1:2.

Synthesis of bulk powder 1. The polycrystalline powder of **1** was prepared by the modified experimental procedure.[21] All of the steps were carried out in ambient conditions. To the suspension of the H_2thpy·⅓H_2O ligand (0.5 g, 3 mmol) in 150 ml of water was added the solution of $NaHCO_3$ (0.125 g, 1.5 mmol) in 5 ml of water. Then a solution of $Fe(NO_3)_3·9H_2O$ (0.626 g, 1.5 mmol) in 50 ml of water was added dropwise with stirring to the solution. The resulting mixture was stirred for 30 min. The black polycrystalline precipitate was isolated by filtration, washed with 10 ml of water, and left to dry at room temperature to a constant weight. Yield: 0.453 g (77%).

Elemental analysis calcd (%) for [Fe^{III}(Hthpy)(thpy)]·H_2O (**1**) ($C_8H_{13}FeN_6S_2O_5$, M_w=393.21 g/mol): C, 24.44; H, 3.33; N, 21.37; S, 16.31; found: C, 24.60; H, 3.34; N, 21.44; S, 16.50. The EPMA of bulk powder **1** afforded the elements in the ratio Fe:S = 1:2.

The powder X-ray diffraction (PXRD) pattern at room temperature of bulk powder **1** is in agreement with the solved structure of crystals **1** (Fig. S2†).

Thermogravimetric analysis (TGA) was performed on bulk sample **1** to monitor the desolvation process (Fig. S3†).A total weight loss of 4.5% (calcd 4.2%) in the temperature range of 368 - 423 K is equivalent to one water molecule in the lattice of complex **1**. The thermogravimetric analysis shows the stability of the ferric complex **1** in the temperature range of magnetic measurements up to 368 K. So, the high-temperature spin-crossover is not caused by loss of water.

Results and discussion

Synthesis

Complex Fe^{III}(Hthpy)(thpy)]·H_2O (**1**) was synthesized by the direct reaction of the H_2thpy ligand with $Fe(NO_3)_3·9H_2O$. The single crystals of **1** were grown at ratio H_2thpy:KOH = 1:2, while the powder precipitate was obtained at ratio H_2thpy:$NaHCO_3$ equal to 2:1. The alkaline solution for the first case shifted the equilibrium between the thione/thiol ~C=S↔~C–S$^-$ forms to the dianionic thiol-form of the H_2thpy ligand, which led to the slow formation of water-insoluble crystals of complex **1** suitable for X-ray diffraction analysis. It is interesting to note that the same deprotonation reaction of the H_2L ligand with lithium hydroxide monohydrate LiOH·H_2O in a ratio of 1:2 produces the anionic complex Li[Fe^{III}(thpy)$_2$]·3H_2O with dianionic thiol-form of ligand at complexation with iron(III).[25]

Infrared spectroscopy

The experimental ATR FT-IR absorption spectra and calculated IR vibration frequencies of the complex **1**, presented in Figure 2, are in a good agreement.

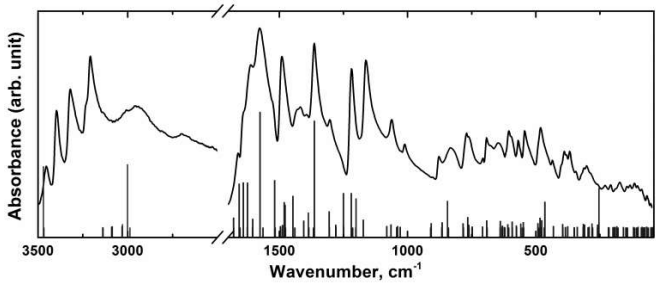

Fig. 2 Experimental ATR FT-IR absorption spectra for $[Fe^{III}(Hthpy)(thpy)]\cdot H_2O$ (**1**) (black line), T = 298 K, without preliminary sample preparation. Calculated (TPSSh/6-311+(d,p)) IR vibrational frequencies of the **A** pair of complex **1** in the LS state (blue bars).

Comparison of experimental ATR FT-IR absorption spectra of the H_2thpy·⅓H_2O ligand and $[Fe^{III}(Hthpy)(thpy)]\cdot H_2O$ complex are presented in Figure S4† The main vibrational bands of the free-ligand and the neutral complex **1** are reported in Table S1†. For both samples, the stretching vibrations of the NH_2 and OH (water and carboxy-) groups appear in the 3500 -3200 cm^{-1} region. The structure of the ligand is altered upon complexation (Fig. S4†) that can be observed through the shift of the characteristic bands. The assignment of bands involving the C=S group in the spectrum of the free- ligand may include bands at 1420, 1256 and 1200 cm^{-1}. The shift (2-17 cm^{-1}) of these bands, the disappearance of absorption at 1256 cm^{-1} and the appearance of a new band at 543 cm^{-1}, attributed to the stretching vibration of the Fe-S groups for the complex **1**. The absence of stretching vibrations of the COO-H and C=N groups in the spectrum of the ferric complex, and detection of new bands at 568 and 543 cm^{-1} that assignment to the stretching vibration of the Fe-O and Fe-N groups respectively, are observed. The appearance of these new bands indicates the coordination of the pyruvic acid thiosemicarbazone ligand to the center iron(III) ion in complex **1**.

The graphical representations of the selected calculated IR vibrational modes for the **A** pair (see crystal structure) of the complex **1** are shown in Table S2†.

Crystal structure

Complex **1** crystallizes in the monoclinic space group $P2_1/n$. The complex is indeed isomorphous with its Cr(III) analogue, as was proposed by Hendrickson in ref. 21. Asymmetric unit contains one formula unit with all atoms in general positions. An ORTEP drawing of **1** at 150 K is shown in Fig. 3, the key bond lengths and angles are listed in Table S3†.

In the 150 K structure, the Fe(III) ion is coordinated by two chelating ligands, one of which is in the protonated monocharged thione form ($Hthpy^-$) while another is in the deprotonated dianionic thiol form ($thpy^{2-}$). The resulting $[Fe^{III}(Hthpy)(thpy)]$ complex is neutral. The ligands in the complex **1** are orthogonal to each other: the angle between the mean thpy planes based on ten non-H atoms ($SO_2N_3C_4$) is 89.39(2) °. Two nitrogen, two oxygen, and two sulfur atoms form the distorted octahedral environment of the Fe center. The coordinated N atoms are in the *trans*-positions relatively to each other, whereas the O atoms and S atoms are in the *cis*-orientation. Fe-X bonds in the octahedron are slightly shorter for the dianionic $thpy^{2-}$ ligand than for the monoanionic $Hthpy^-$ one, the maximum difference of ~0.03 Å is observed for Fe-O bonds (Table S3†).

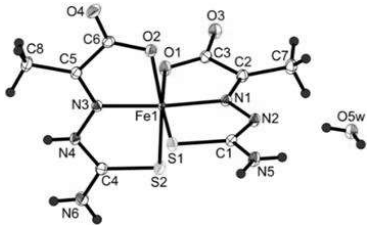

Fig. 3 The asymmetric unit in **1** at 150K with the atom numbering scheme (ORTEP drawing, thermal ellipsoids at a 50% probability level).

The average Fe-N, Fe-O and Fe-S bond lengths at 150 K are 1.912(3), 1.946(15) and 2.231(5) Å, respectively. These values are comparable to similar values in the $Li[Fe^{III}(thpy)_2]\cdot 3H_2O$ structure[25] and correspond to the low-spin state of complex **1**. Small distortion of the coordination Fe(III) octahedron is additional evidence of the LS state: the O-Fe-S and N-Fe-N angles are close to 180 °, and the distortion parameter Σ, which is a measure of the angular deviation from a normal octahedral geometry, is equal to 52.8 ° (Table S4†).

The Fe complex is neutral in **1** and anionic in $Li[Fe(thpy)_2]\cdot 3H_2O$.[25] It is found that in the neutral complex the average Fe-O bond is noticeably shorter: 1.946(15) Å in $[Fe^{III}(Hthpy)(thpy)]^0$ vs. 1.974(4) Å in $[Fe^{III}(thpy)_2]^-$. At the same time, the difference in the Fe-N, Fe-S bond lengths is an order of magnitude smaller (~0.001-0.004 Å) and opposite in sign.

The crystal packing contains infinite chains of the Fe(III) complexes running along the *c*-axis (Fig. 4). Two types of interactions (**A** and **B**) between the adjacent complexes alternate along the chain. In both interactions, there is π-stacking of parallel planes of equivalent ligands related by inversion symmetry. In the interaction **A**, the monoanionic $Hthpy^-$ moieties are stacked (they are marked by black bonds in Fig. 4 and 5). The corresponding Fe…Fe distance of 6.1534(3) Å is the shortest in the structure **1**. However, the mean planes of $Hthpy^-$ ligands (including all 10 non-H atoms) are well separated from each other at the distance of 4.70(5) Å and between them there are no shortened interatomic contacts.

The complexes in the interaction **A** are connected only through a pair of equivalent $N\text{-}H_{Hthpy}\cdots O_{thpy}$ bonds from the –NH function of $Hthpy^-$ to non-coordinated oxygen of $thpy^{2-}$, H…O distance is 2.07 Å (Fig. 5).In **B**, a π-π interaction exists between the dianionic $thpy^{2-}$ ligands (white bonds in Fig. 4 and 5). In spite of the larger Fe…Fe distance of 7.0599(4) Å, the separation of $thpy^{2-}$ planes is 3.17(5) Å and several N…N and C…N contacts of 3.238(2)-3.370(2) Å are formed (black dotted lines in Fig. 4 and 5).

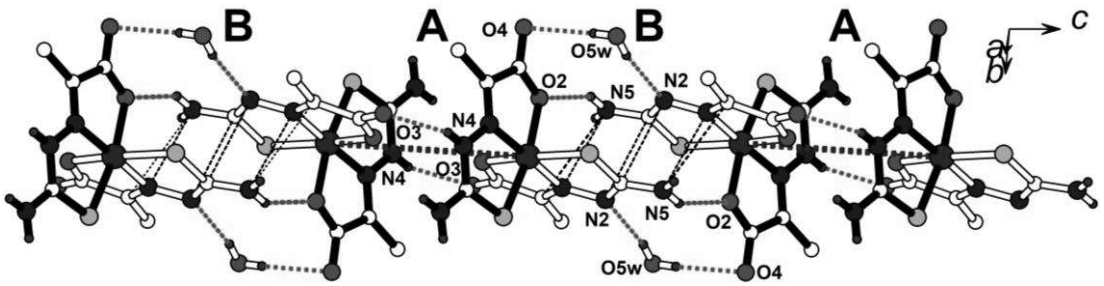

Fig. 4 Chain of the Fe complexes with π-stacking of the Hthpy$^-$ ligands (black bonds, interaction **A**) and thpy^{2-} ligands (white bonds, interaction **B**). Fe…Fe distances along the chain are 6.1534(3) Å (brown dashed lines) and 7.0599(4) Å.

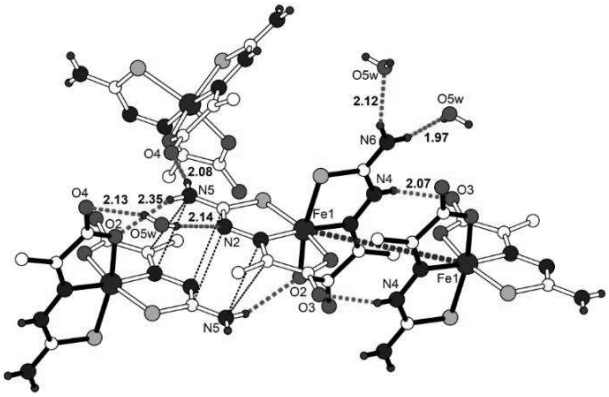

Fig. 5 Hydrogen bonding in the structure **1**. N-H…O and O-H…N/O bonds are shown by red dashed lines, H…N/O distances are given in Å. Shortened N…N and C…N contacts are shown by black dotted lines.

Similar π-stacking of the thpy^{2-} ligands was observed in the anionic Li[Fe^{III}(thpy)$_2$]·3H$_2$O complex, with the shortest in this structure Fe…Fe distance of 6.7861(4) Å.[25] The π-stacking in the interaction **B** in **1** is enhanced by paired hydrogen bonds N-H$_{thpy}$…O$_{Hthpy}$ from -NH$_2$ group of thpy^{2-} to the coordinated oxygen of Hthpy$^-$ (H…O 2.35 Å) and indirect H-bonding through H$_2$O molecule (Fig. 4 and 5). O-H$_{water}$…N$_{thpy}$ and O-H$_{water}$…O$_{Hthpy}$ bonds are formed with deprotonated N atom of thpy^{2-} and non-coordinated O atom of Hthpy$^-$; corresponding H…N/O distances are 2.14(2)/2.13(2) Å. The closest Fe…Fe distance between the chains is 6.5418(4) Å.

The compound **1** includes one crystallized water molecule, which is well fixed in the structure by hydrogen bonding. The H$_2$O molecule participates in four different hydrogen bonds with four surrounding Fe complexes and acts in these interactions both as H-bond donor and H-bond acceptor (Fig. 5). Details of hydrogen bond geometry at 150 K are given in Table S5†.

The temperature behavior of the structure **1** was investigated by a single crystal X-ray diffraction technique in the range of 150-364 K (Table S6†). All the experiments were performed on one single crystal during the heating, complete structural analysis was done at 350 K to compare the details with the low temperature data (Tables S3-S7†). It is found that between 150 and 350 K the crystal retains [Fe^{III}(Hthpy)(thpy)]·H$_2$O composition and monoclinic $P2_1/n$ symmetry. Fig. 6 represents temperature dependences of the unit cell parameters. The *a* and *c* parameters and β angle increase as temperature rises, whereas the *b* axis length has a minimal value at 250 K, and the reason for this is unclear. Upon heating, all Fe-X distances become slightly longer but still point to the LS geometry of Fe(III) at 350 K (Table S3†). The average Fe-N, Fe-O and Fe-S bond lengths at 350 K are 1.923(2), 1.948(15) and 2.238(10) Å, respectively.

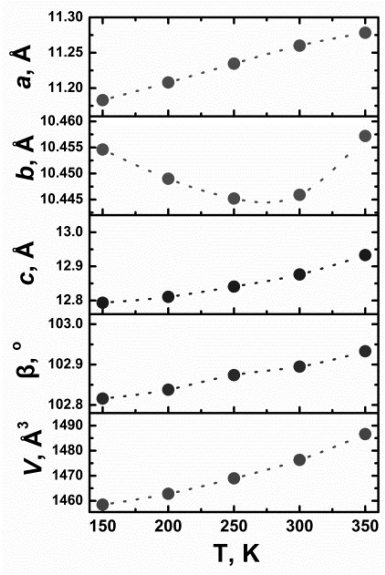

Fig. 6 Temperature dependences of unit cell parameters of the single crystal **1**.

The lengthening of the bonds from 150 to 350 K does not exceed 0.6%. The distortion of the FeN$_2$O$_2$S$_2$ octahedron also slightly increases at 350 K in comparison with the 150 K structure (Table S4†). More careful and slow heating of another crystal above 350 K showed that the structure still exists at 360 K, but the crystals are destroyed at 364 K (Fig. S1†). At 360 K the geometry of the Fe complex corresponds to the LS state, but bond lengths could not be directly compared for the first and second crystals. This allows us to conclude that the phase transition is very abrupt and occurs between these temperatures (see Magnetic section).

Magnetic measurements

Dc magnetization and X-band EPR spectroscopy

The temperature dependence χT of the product is shown in Figure 7. Three ranges can be selected for the temperature dependence of the χT of complex **1**: 2–60 K (1st), 60–300 K (2nd), and 300–363 K (3rd).

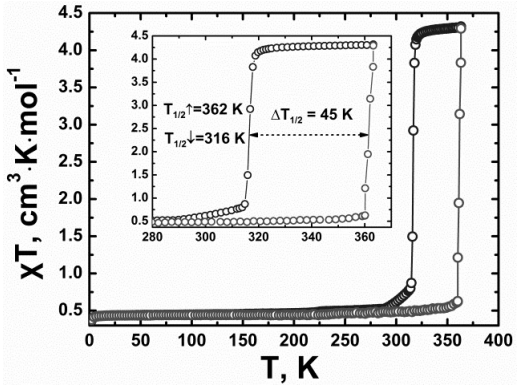

Fig. 7 Temperature dependences of χT in the heating (red circles) and cooling (blue circles) modes for [Fe^{III}(Hthpy)(thpy)]·H_2O according to *dc* magnetic measurements. The inset shows the enlarged region of the hysteresis loop. The scan rate is 2 K/min.

In the first temperature range below 60 K, the values of χT abruptly decrease from 0.436 cm³·K·mol^{-1} to 0.378 cm³·K·mol^{-1} at 2 K for heating and cooling modes. This feature is attributed to the onset of the antiferromagnetic correlations between neighboring iron(III) centers. Based on the X-ray data, the crystal structure of **1** consists of interconnected dimer pairs of [Fe^{III}(Hthpy)(thpy)] complex through short contacts (see Fig. 4 and 5). One formula unit of complex **1** accounts for half of the dimer (pair **B**, Fig.4). Thus, the Bleaney–Bowers equation for a model of an isolated [Fe^{III}(Hthpy)(thpy)] dimer χ_{iso} (eqn (1)) was applied to fit the experimental data in the heating mode in the temperature range of 2–60 K without the spin-crossover process (the solid line in the Fig. S5†).[26]

$$\chi_{iso} = \frac{N_a \cdot g_{LS}^2 \cdot \mu_b^2}{k_b \cdot T} \cdot \frac{1}{3 + e^{\frac{-2 \cdot J}{k_b \cdot T}}} \quad \text{(Eqn. 1)}$$

where g_{LS} is the spectroscopic splitting factor applicable to the $^2T_2$ (LS, S = 1/2) state; *Na*, μ_b and k_b are the Avogadro, Bohr and Boltzmann constants; *T* is the temperature in Kelvin; and *J* is the intra-dimer coupling constants. The best fitted curve parameters are g_{LS}=2.165(1); J/k_B= − 0.498(1) K. The determination coefficient for the proposed model is R^2=0.996

The resulting value of g_{LS} ≈2.17 (g > 2) is typical of the LS configuration of iron(III) with spin–orbit interaction.[27] The J/k_B = − 0.498(1) K exchange constant denotes the weak antiferromagnetic exchange between the iron(III) centers in the dimer pairs **B** of **1** due to the bulky Hthpy$^-$ and thpy^{2-} ligands acting as mediators of superexchange. It is worth noting that the DFT calculations of the optimized structure of two isolated [Fe^{III}(Hthpy)(thpy)] complexes also correctly predict a weak exchange J(calc) = − 0.92 K. It should be noted that the application of the Curie–Weiss law gives an overestimated χT value of ~0.005 cm³·K·mol^{-1} at 2 K in comparison with the eqn (1) (see Fig. S6†).

On the second temperature range in 60–300 K, the values of χT gradually increase from 0.440 cm³·K·mol^{-1} to 0.483 cm³ K mol^{-1}. This slight and gradual decrease in χT can be attributed to the appearance of the high spin phase. The concentration of the HS phase (γ_{HS}) at 300 K can be estimated at ~2.7%.

For the third temperature range in 300–363 K, complex **1** demonstrates an abrupt one-step spin-crossover in narrow temperature range with wide hysteresis loop 45 K (Fig. 7 and S7†). In heating mode, the values of χT gradually increase up to 0.600 cm³ K mol^{-1} at 360 K, which corresponds to the γ_{HS}= 4%. Then, the values of χT abrupt increase from 0.600 to 4.318 cm³ K mol^{-1} in the narrow temperature range of 360–363 K. The χT=4.318 cm³ K mol^{-1} at 363 K corresponds to HS (S=5/2) Fe(III) with g_{HS}= 1.987. The half-transition temperature in heating mode is equal to $T_{1/2}\uparrow$ =361 K, which reasonably agrees with the maximum of 1st derivative of χT *vs* T at 360 K (Fig. S7†).

After a complete SCO at 363 K, the χT gradually decreases to 4.137 cm³ K mol^{-1} at 320 K, which corresponds to the decrease of $\Delta\gamma_{HS}$=5 %. Next, the values of χT rapidly decrease to approximately constant value 0.516 cm³ K mol^{-1} (γ_{HS}≈2 %) at 285 K. A slow decrease from 0.516 to 0.439 cm³ K mol^{-1} is also observed in the range 285–100K, corresponding to a return to a pure LS Fe(III) with g_{LS} ≈2.17 after a complete SCO. The half-transition temperature in cooling mode is equal to $T_{1/2}\downarrow$ =316 K, which also agrees with the maximum of 1st derivative of χT *vs* T at 317 K (Fig. S7†). Thus, the average temperature is equal to $T_{1/2}$=½·($T_{1/2}\downarrow$ +$T_{1/2}\uparrow$)≈340 K.

The hysteresis spectra of EPR for **1** during the heating cycle (*left*) and cooling cycle (*right*) in the temperature range of 300-368 K are shown in Figure 8.The line position (g-factor 2.12) and form of the line shape are typical for Fe(III) complexes, and correspond to a low-spin state Fe(III) ion. At temperatures 100-315 K, Curie's law only shows a change in the line intensity. However, upon subsequent heating (Fig. 9), two distinct temperature ranges can be identified. The first heating range, 315-355 K, displays a deviation from Curie's law.

The second range, 355-368 K, exhibits a sharp decrease in the integral intensity due to a rapid transition to a high-spin state Fe(III) ion in the complex **1**. Upon cooling, a stable HS state is observed in the temperature range of 368-346 K. The concentration of the low-spin state sharply increases from 346-332 K, followed by a slow transition process to the LS state with full recovery of the initial EPR spectrum line intensity, which ends at 315 K.

The line noticeably broadens in the temperature range of 315-368 K. Therefore, dependence of the integral intensity of the EPR spectra (double integration) was examined (Fig. 9). The integral intensity multiplied by temperature is selected on the Y-axis, similar to *dc* magnetic measurements. In this case, Curie's law dependence corresponds to a horizontal line.

A temperature hysteresis is clearly observed between data recorded during both heating and cooling modes, starting at around 357 K and 342 K, respectively. These observations are in line with *dc* magnetic measurements, and the sensitivity of this hysteresis to the heating and cooling rate should be taken into account.[2]

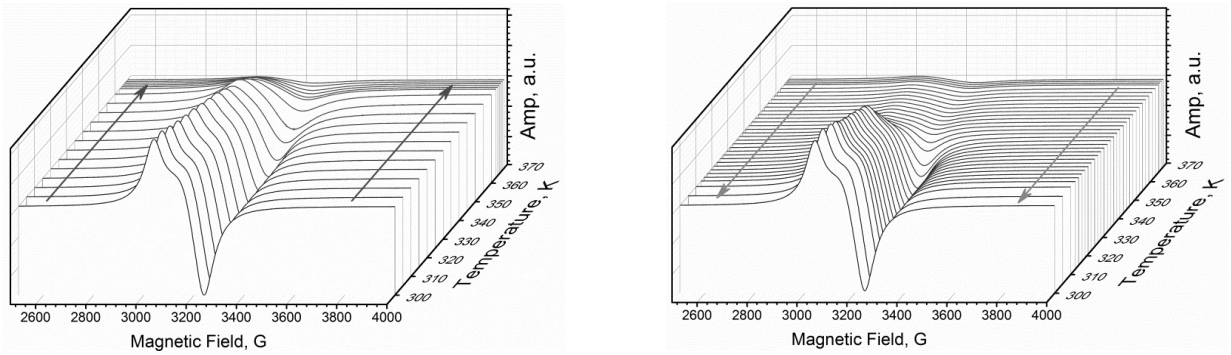

Fig. 8 Hysteresis of EPR spectra of $[Fe^{III}(Hthpy)(thpy)]\cdot H_2O$ during the heating (left) and cooling (right) cycle depending on the temperature 300–368 K.

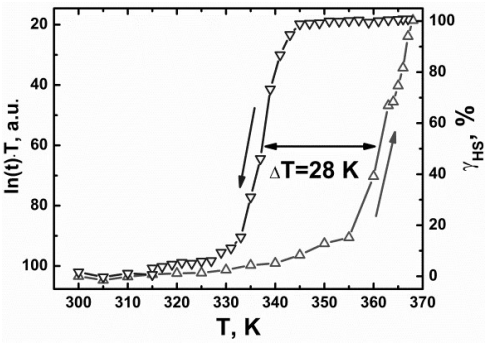

Fig. 9 Hysteresis of product of EPR signal integral intensity on temperature (*left axis*)/ γ_{HS} (*right axis*) from temperature during the cycle of heating (red triangles up) and cooling (blue triangles down) in the temperature range 300–368 K for the complex **1**.

The complex $[Fe^{III}(Hthpy)(thpy)]\cdot H_2O$ saves its composition up to 370 K (see Experimental section), so the measurements were carefully performed below this temperature. Thus, the high-temperature spin transition is not caused by water loss.

^{57}Fe Mössbauer spectroscopy

Complex **1** was further characterized by ^{57}Fe zero-field Mössbauer spectroscopy in the temperature range of 80–365 K at cooling and heating modes (Fig. 10 and 11). Mössbauer spectroscopy data are in agreement with *dc* magnetic measurements.

The spectra of **1** show one slightly asymmetric quadrupole doublet of LS Fe(III) in the temperature range of 80–361 K at heating mode. The Mössbauer parameters of spectrum at 296 K are ΔE_Q=3.073(2) mm/s, δ=0.127(1) mm/s, Γ_-=0.326(5) mm/s and Γ_+=0.270(4) mm/s (Table S8†). It is worth noting that the slight asymmetries and parameters of spectra at 296 K for neutral complex $[Fe^{III}(Hthpy)(thpy)]\cdot H_2O$ and $[Fe^{III}(thpy)_2]^-$ anionic complex in salt $Li[Fe^{III}(thpy)_2]\cdot 3H_2O$ (ΔE_Q=3.205(4) mm/s, δ=0.144(2) mm/s, Γ_-=0.354(2) mm/s and Γ_+=0.312(2) mm/s) are close to each other.[25] The large value of isomeric shift for anionic complex $[Fe^{III}(thpy)_2]^-$ ($\Delta\delta$=0.144(2)-0.127(1)=0.017(2) mm/s), compared to complex **1**, is associated with large Fe-O distances that leads to higher electron density in the 4s shell of iron(III). In addition, it should be noted that $[Fe^{III}(Hthpy)(thpy)]$ complex unlike $[Fe^{III}(Hthpy)(thpy)]\cdot H_2O$ complex has a symmetrical LS quadrupole doublet at room temperature.[21] It is clear that spin-spin relaxation is dominant in these neutral Fe(III) complexes based on pyruvic acid thiosemicarbazone ligand, because the asymmetry in the low-spin doublet is closely related to the inclusion of water molecules in the crystal structure.[28]

In the narrow temperature range of 361–365 K, the abrupt SCO is observed. At 363 K, HS and LS quadrupoles are distinct since spin state interconversion rate is slow relative to the Mössbauer timescale.[29] The ratio of HS fraction is equal to γ_{HS}=68% at this temperature. The opposite asymmetries of doublets for HS and LS states are due to the opposite sign of quadrupole splitting. The LS state has the main contribution to ΔE_Q from Fe(III) electronic shell, which may have a sign opposite to the contribution of localized charges by the octahedral environment of Fe(III) in HS state. A similar change in the asymmetry of HS and LS quadrupole doublets during the spin-crossover was also noted for $N_2S_2O_2$-coordination anionic complex Fe(III) based on 5Cl- salicylaldehyde thiosemicarbazone ligand in $K[Fe^{III}(5Cl\text{-}thsa)_2]$ salt.[30]

One asymmetric HS quadrupole doublet of Fe(III) [ΔE_Q=0.95(1) mm/s, δ=0.327(7) mm/s, Γ_-=0.54(2) mm/s and Γ_+=0.94(4) mm/s] indicating a complete SCO is observed at 365 K. Taking into account the fact of the crystal destruction above 364 K, it can be assumed that the SCO in complex **1** leads to a significant increase of Fe...Fe distances in crystal structure.

Thus, the increase of intermolecular Fe...Fe distance leads to the increase of asymmetry for HS doublet. Spin-spin relaxation is dipolar in nature, and therefore it is attenuated with an increase in intermolecular Fe...Fe distance.[28, 31]

In cooling mode, the preservation of HS state is observed in spectra at 365 K, 353 K and 333 K. The HS and LS quadrupole doublets are detected in the spectrum at 328 K with γ_{HS}=76% ratio. At 323 K, the ratio of HS fraction decreases abruptly to γ_{HS}=15%. The HS doublet completely disappears upon cooling to room temperature. Thus, the temperature hysteresis loop of 35 K in changes of the γ_{HS} concentration is detected during heating and cooling modes. This value is 10 K lower compared to *dc* magnetic measurements. It is clearly associated with the difference in conditions of the measurements. As a result, the hysteresis loop narrows.[32, 33]

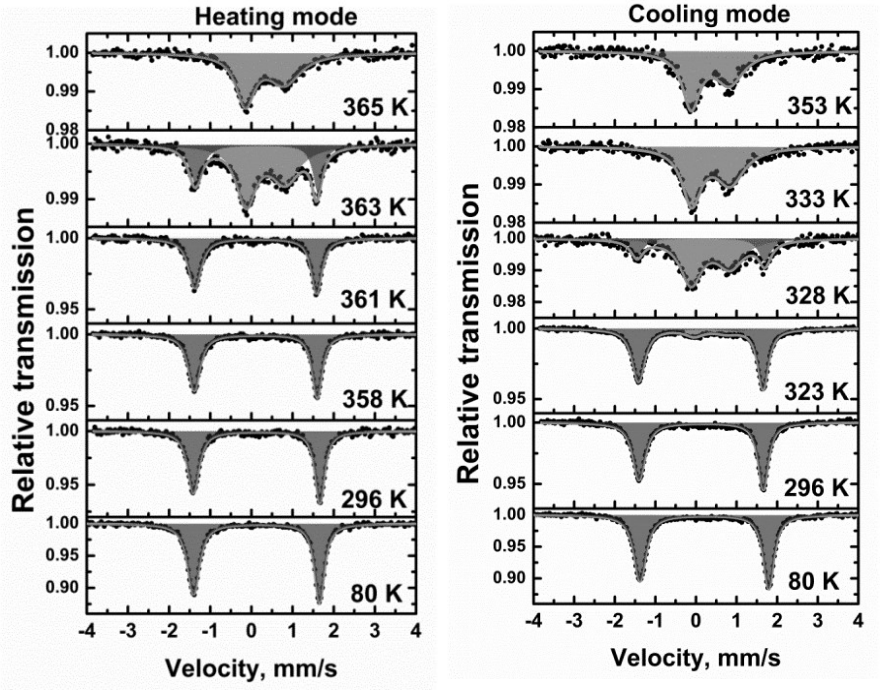

Fig. 10 Mössbauer spectra of $[Fe^{III}(Hthpy)(thpy)]\cdot H_2O$ at heating and cooling modes in temperature range 80–365 K. An area of doublet highlighted in red corresponds to HS (S=5/2) Fe(III), whereas area of doublet highlighted in blue corresponds to the LS state. Green line denotes fit line.

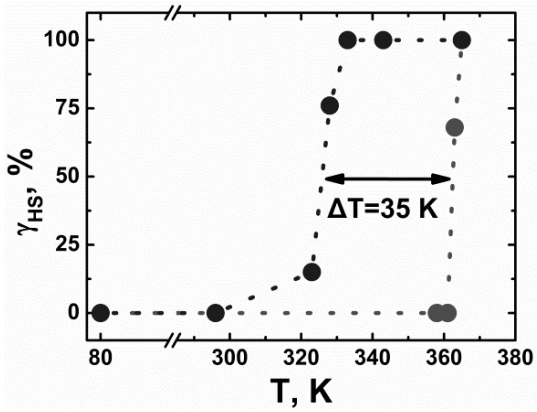

Fig. 11 The ration of γ_{HS} in % obtained from Mössbauer spectra of $[Fe^{III}(Hthpy)(thpy)]\cdot H_2O$ in heating and cooling modes in temperature range 80–365 K. The temperature-axis contains a break.

It is important to note the broadening of the lines of the LS quadrupole doublet in the spectra at 296 and 80 K in cooling mode after SCO compared to heating mode before SCO by ~0.03–0.04 mm/s (Table S8†). The broadening of the lines is consistent with a decrease of sample crystallinity.[34]

Even a slight heating of complex **1** above the temperature of crystalline water loss, for example 373 K, is reflected in the Mössbauer spectra by the appearance of a symmetrical HS quadrupole doublet at 80 and 296 K (Fig. S8†, Table S9†). Thus, Figure 10 clearly shows that complex **1** retains its composition during high-temperature Mössbauer measurements in the range 80-365 K.

So, complex **1** demonstrates a full abrupt SCO above room temperature with a wide hysteresis loop 45 K and $T_{1/2}$=340 K according to *dc* magnetic measurements. The antiferromagnetic exchange is realized below 50 K due to the dimeric structural motif and the short contacts in the crystal structure.

DFT calculation

DFT calculations of the $[Fe^{III}(Hthpy)(thpy)]$ complex

DFT calculations of the isolated neutral complex $[Fe^{III}(Hthpy)(thpy)]$ as well as the **A** and **B** pairs in structure were carried out to establish the relationships between the crystal structure and magnetic behavior. Calculations devoted selection of a functional correctly predicting the parameter of the energy gap between the HS and LS states were performed earlier in ref. 25. A comparison of the electronic structure features of anionic and neutral Fe(III) complexes with $N_2S_2O_2$ coordination was presented in ref. 25 and 35. The well-established TPSSh functional was chosen for calculations of the geometry of structural units and the exchange interaction parameter using the BS method.[36, 37]

The key parameters of the optimized geometries of **A** and **B** pairs were compared with the calculated geometry of the isolated complex and the crystal structure at 150 K (Fig. 12). The data allow us to conclude that the gas-phase optimized geometries of **A** and **B** pairs differ from the experimental values by < 0.1 Å (Table S10†).

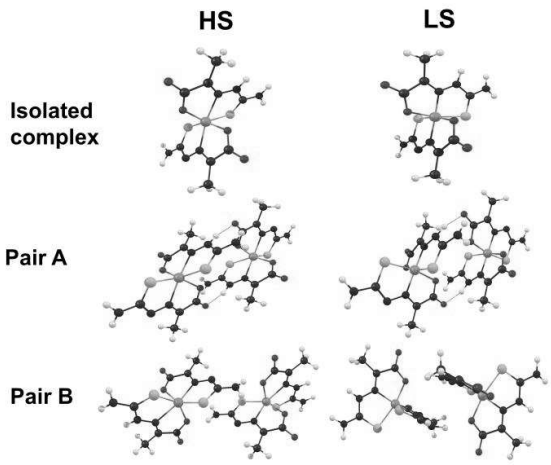

Fig. 12 Optimized geometries of isolated neutral complex [Fe^{III}(Hthpy)(thpy)], **A** and **B** pairs of complexes calculated at the TPSSh/6-311+G(d,p) level in HS (left) and LS (right) states. Blue dotted line denotes hydrogen bond. Color code:, H, white; C, black; S, yellow; Fe, orange; N, blue; O, red.

Due to the destruction of the crystal of complex **1** at the SCO it was not possible to establish the structure in the HS state (see structural and magnetic part, Fig. S1†). To clarify the reasons of this phenomenon, the comparison of the selected parameters of two structural fragments of **A** and **B** pairs of neutral complexes [Fe^{III}(Hthpy)(thpy)] in the HS and LS states was carried out (Tables S11† and S12†). Analysis of the changes in bond lengths of the Fe(III) coordination octahedron in two spin states showed that the relative elongation values increase in the series Fe–O(~4%)→ Fe–S(~8%)→ Fe–N_{im}(~14%).

Comparison of the calculated Fe...Fe distances for **A** and **B** pairs in the LS state with the experimental values showed a difference of 0.0452(4) Å and 0.1559(4) Å, respectively. The negligible difference between the experimental and calculated values for the **A** pair confirms the high degree of H-interaction between the two complexes. For the **B** pair, this difference is higher, which demonstrates the significant influence of crystal packing on the formation of π-π interactions between two adjacent complexes via the $thpy^{2-}$ forms of the ligand.

Based on the DFT calculations, it can be assumed that the significant increase in the Fe...Fe distance for the **A** pair during the spin-crossover by ~14% leads to increasing the unit cell parameters with crystal destruction above 364 K (see Structural section, Fig. S1†).

Exchange coupling constants from broken-symmetry DFT

According to *dc* magnetic measurements, the crystal structure of [Fe^{III}(Hthpy)(thpy)]·H_2O contains magnetic exchange interactions in **B** pairs of neutral complexes, which are formed through interactions of two $thpy^{2-}$ ligands (see structural section). Previously, this type of π-π interaction of the $thpy^{2-}$ ligand forms was identified between pairs of anionic complexes [Fe$(thpy)_2]^-$ in the structure of Li[$Fe^{III}(thpy)_2$]·$3H_2O$ salt.[25]

The Heisenberg spin Hamiltonian shown in the equation $H = -2J_{12}\widehat{S_1}\cdot\widehat{S_2}$ was applied for the analysis, where J_{12} is the magnetic coupling between the unpaired electrons in sites 1 and 2. The negative value of J corresponds to the antiferromagnetic interaction. In the case of weak exchange interaction, Noodleman[38] (eqn (2)) and Yamaguchi[39] (eqn (3)) were used to estimate the parameter J from the energies of the TS and BS states:

$$J_N = -\frac{E_{TS} - E_{BS}}{4S_1S_2} \qquad \text{(Eqn. 2)}$$

$$J_Y = -\frac{E_{TS}-E_{BS}}{<S_{TS}^2>-<S_{BS}^2>} \qquad \text{(Eqn. 3),}$$

where $< S_{TS}^2 >$ and $< S_{BS}^2 >$ are the total spin angular momenta of the TS and BS states.

The calculated exchange interaction parameters for the fully optimized **B** pairs geometry as well as the **B** pairs fragment with optimized hydrogen atoms correctly predicted the antiferromagnetic nature, but greatly overestimated the experimental values of *J* (Table S13†). To study the influence of small geometric modifications on the calculated exchange interaction constant, the *J* values for the geometry of **B** pair were also calculated directly from the X-ray structure at 150 K. These calculations demonstrate the value of the exchange interaction parameter J_N=J_Y= − 0.92 K, which correctly predicts the weak antiferromagnetic nature of the interaction between Fe(III) centers and are in good agreement with experimental data *J(exp)*= − 0.498(1) K (Table S13†).Thus, it can be concluded that in this case, the small geometric modifications of the structural fragment of the **B** pair significantly influence the parameter of the exchange coupling constant *J*.

To confirm the exchange path between magnetic centers, the change in the Mulliken spin density during the transition from the TS state to the BS state was analyzed (Fig. 13 and 14).

Iron atoms in the TS and BS states have the same absolute value of spin density equal to 1.029. Coordinated nitrogen atoms (N_{im}) have the opposite sign compared to the iron atom in the TS state ρ = − 0.057, and in the BS state ρ = ±0.059, respectively. On the opposite, the coordinated sulfur atoms with ρ = ±0.042 have the same sign as the iron atom in both states. The change in spin density from the TS state to the BS state indicates the participation of nitrogen atoms in magnetic exchange, in contrast to sulfur atoms. The nitrogen and carbon atoms from the N=C fragment in the TS state have values of ρ(N) = 0.007 and ρ(C) = 0.004 coincided in sign, which are opposite in sign to the nitrogen atom (N_{im}) from the coordination sphere in turn. In the BS state, the spin densities of the nitrogen and carbon atoms of the N=C fragment equaled to ρ (C) = ±0.007 and ρ(N) = ±0.009 also coincide with each other, and these values are also opposite in sign to the nitrogen atom from the coordination sphere.

Thus, the change of spin density from the TS state to the BS state for the N=C fragment and coordinated nitrogen atom (N_{im}) also directly indicates the polarization competition between two iron atoms with α- and β-spin density (Fig. 13), respectively.[40,41] In the case of π-π bonded pairs of neutral complexes [Fe^{III}(Hthpy)(thpy)], the exchange pathway with 4 intermediaries can be represented as the scheme Fe(1.029) ↔ N_{im}(-0.059) ↔ [N(0.009)=C(0.007)]···[C(-0.007)=N (-0.009)] ↔ N_{im}(0.059) ↔ Fe(-1.029).

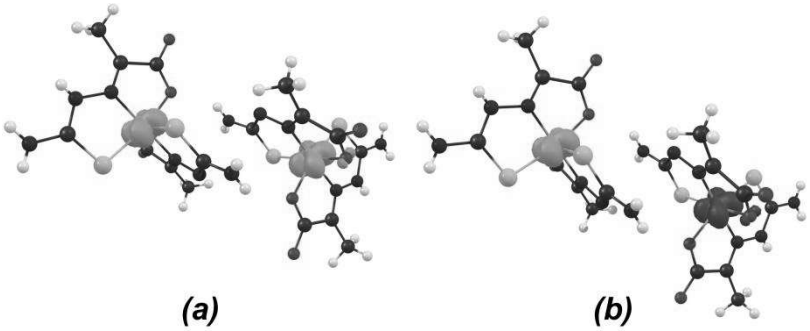

Fig. 13 Spin density plots of π-π bonded [Fe^{III}(Hthpy)(thpy)] neutral complexes (**B** pairs) corresponding to the TS (*a*) and BS (*b*) states: red, positive spin density (α) and purple, negative spin density (β). The isodensity surfaces are plotted with the cut-off values of 0.01 e·Å^{-3} for the TS and BS states. The TPSSh functional with the 6-311+G(2df,2p) basis was used.

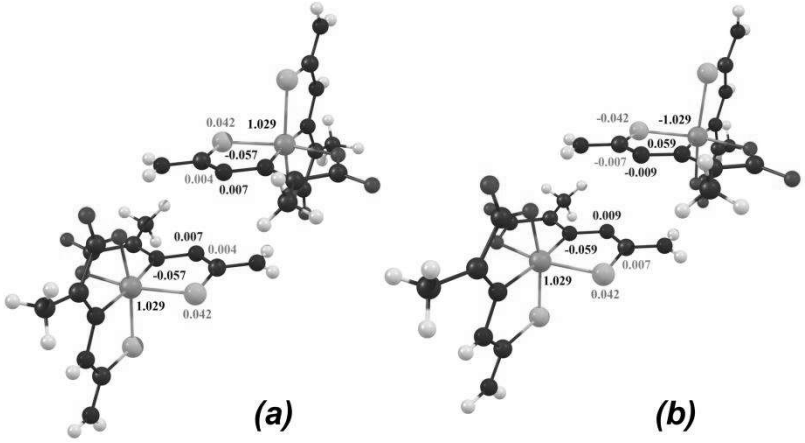

Fig. 14 DFT-calculated net Mülliken spin densities for selected atoms in the TS (*a*) and BS (*b*) states of π-π bonded [Fe(Hthpy)(thpy)] neutral complexes (**B** pairs). The color of the spin density value corresponds to the color of the atom. The TPSSh functional with 6-311+G(2df,2p) basis set was used.

Conclusions

The X-ray structure of the hydrate of the neutral iron(III) complex with pyruvic acid thiosemicarbazone ligand [Fe^{III}(Hthpy)(thpy)]·H_2O (**1**) has been determined for the first time. The crystals of complex **1** were grown at ratio H_2thpy:KOH 1:2, while the powder precipitate was obtained at ratio H_2thpy:$NaHCO_3$ equal to 2:1. Complex **1** crystallizes in monoclinic space group $P2_1/n$. The molecules in crystal packing **1** are arranged in π-π bonded pairs where halves of pair is linked together by hydrogen bonds. Crystallization water molecules are located in cavities between the extended chains of neutral complexes, which leads to the formation of hydrogen bonds net in the structure and the creation of additional bonds between the iron(III) centers. According to the analysis of the crystal structure at 150 and 350 K, the iron(III)-ligand bond lengths correspond to the LS state of the magnetic center.

According to *dc* magnetic measurements, a complete abrupt spin-crossover with $T_{1/2}$=340 K and the hysteresis loop of 45 K occurs in the temperature range of 300–363 K. The existence of a wide hysteresis loop for SCO complex **1** was also confirmed by high-temperature EPR and Mössbauer spectroscopy measurements. Based on the X-ray structure, the Bleaney–Bowers equation for the isolated dimer model (S=1/2) was used to approximate the temperature dependence of the magnetic susceptibility in the range of 2–50 K. The experimental constant of intradimer coupling J/k_B= −0.498(1) K corresponds to a weak antiferromagnetic exchange between the magnetic centers of iron(III). The negligible values of the exchange interactions between Fe(III) centers can be explained by the presence of six intermediaries participating in magnetic exchange.

Based on DFT calculations, it can be assumed that the significant calculated increase of ~14% in the Fe...Fe distance for the H-bonded halves of π-π bonded **B** pairs during the spin-crossover leads to the crystal destruction above 364 K. In addition, BS-DFT calculations confirm the presence of a weak antiferromagnetic exchange J_N=J_Y= − 0.92 K in **B** pairs of complex **1**, which is in good agreement with the experimental value J_{exp}=–0.498(1) K. Based on the Mulliken spin density distribution, the superexchange pathway between magnetic centers of iron(III) was determined via π-π interaction of C=N fragments of the doubly deprotonated form of the ligand thpy^{2-}. It can be assumed that the formation of π-π bonded pairs through the double deprotonated form of the ligand is a structural feature of neutral and anionic thpy-complexes.

The results described in the article shed light on the class of neutral spin-crossover iron(III) complexes based on the pyruvic acid thiosemicarbazone ligand with the property of abrupt transition and wide hysteresis loop of magnetic susceptibility, which can be applied in modern materials for spintronics.

Author contributions

The synthesis and characterizations of compounds, M.B., N.S., and A.L.; X-ray analysis and crystal structure description, L.Z. and S.S.; *dc* magnetic measurements, K.Z., A.V.; EPR measurements, A.A.; measured and contributed to analyses of ^{57}Fe Mössbauer spectral data and the DFT calculations, M.B.; writing the original draft, M.B., N.S.. All authors discussed the results and contributed to the final manuscript.

Conflicts of interest

There are no conflicts to declare.

Data availability

The datasets supporting this article have been uploaded as part of the ESI,† or at **https://doi.org/ 10.1039/x0xx00000x**.

Acknowledgements

This work was partially supported by the Ministry of Science and Higher Education of the Russian Federation: M.B., N.S., A.L., A.A. (State task, state registration no. 124013100858-3); L.Z. and S.S. (the structural study was carried out within the state assignment for the ISSP RAS).

Elemental, TG analysis, ^{57}Fe Mössbauer and EPR spectra were performed using the equipment of the Multi-user Analytical Center of FRC PCP MC RAS. The authors kindly acknowledge assistance from the Computational Center of FRC PCP MC RAS. PXRD study was made using equipment of the shared facility centre of ISSP RAS.

References

1 Spin-Crossover Materials: Properties and Applications, ed. M. A.Halcrow, *John Wiley & Sons Ltd.*, Chichester, 2013.
2 P. Gütlich and H. A. Goodwin, *Top. Curr. Chem.*, 2004, **234**, 1.
3 A. Hauser, *Top. Curr. Chem.*, 2004, **233**, 49.
4 D. Vidal, J. Cirera and J. Ribas-Arino, *Dalton Trans.*, 2021, **50**, 17635.
5 D. Vidal, J. Cirera and J. Ribas-Arino, *Phys. Chem. Chem. Phys.*, 2023, **25**, 12490.
6 D. J. Harding, P. Harding and W. Phonsri, *Coord. Chem. Rev.*, 2016, **313**, 38.
7 S.-Z. Zhao, H.-W. Zhou, C.-Y. Qin, H.-Z. Zhang, Y.-H. Li, M. Yamashita and S. Wang, *Chem. – Eur. J.*, 2023, **29**, e202300554.
8 A. Tsukiashi, M. Nakaya, F. Kobayashi, R. Ohtani, M. Nakamura, J. M. Harrowfield, Y. Kim and S. Hayami, *Inorg. Chem.*, 2018, **57**, 2834.
9 V. V. Zelentsov, A. V. Ablov, K. I. Turta, R. A. Stukan, N. V. Gerbeleu, E. V. Ivanov, A. P. Bogdanov, N. A. Barba and V. G. Bodyu, *Russ. J. Inorg. Chem.*, 1972, **18**, 1929. (Engl. Transl.)
10 P. Gütlich and H. A. Goodwin, *Top. Curr. Chem.*, 2004, **233**, 1.
11 I. Šalitroš, N. T. Madhu, R. Boča, J. Pavlik and M. Ruben, *Monatsh Chem*, 2009, **140**, 695.
12 Y. Zhang, R. Torres-Cavanillas, X. Yan, Y. Zeng, M. Jiang, M. Clemente-León, E. Coronado and S. Shi, *Chem. Soc. Rev.*, 2024, **53**, 8764.
13 K. S. Kumar and M. Ruben, *Coord. Chem. Rev.*, 2017, **346**, 176.
14 A. Miyawaki, K. Eda, T. Mochida,T. Sakurai, H. Ohta, T. Nakajima and K. Takahashi, *Inorg. Chem.*, 2021, **60**, 12735.
15 W. Phonsri, V. Martinez, C. G. Davies, G. N. L. Jameson, B. Moubarakia and K. S. Murray, *Chem. Commun.*, 2016, **52**, 1443.
16 S. Murata, K. Takahashi, T. Mochida, T. Sakurai, H. Ohta, T. Yamamoto and Y. Einaga, *Dalton Trans.*, 2017, **46**, 5786.
17 S. Floquet, E. Rivière, K. Boukheddaden, D. Morineau, M.-L. Boillot, *Polyhedron*, 2014, **80**, 60.
18 Z.-Y. Li, Y.-Y. Wu, Y. Li, J.-H. Wang, A. Sulaiman, M. K. Javed, Y.-C. Zhang, W. Li and X.-H. Bu, *CCS Chem.*, 2023, **5**, 412.
19 W. Phonsri, D. S. Macedo, B. Moubaraki, J. D. Cashion and K. S. Murray, *Magnetochemistry*, 2016, **2**, 3.
20 S. Padhyé and G. B. Kauffman, *Coord. Chem. Rev.*, 1985, **63**, 127.
21 M. D. Timken, S. R. Wilson and D. N. Hendrickson, *Inorg. Chem.*, 1985, **24**, 3450.
22 E. W. T. Yemeli, G. R. Blake, A. P. Douvalis, T. Bakas, G. O. R. Alberda van Ekenstein and P. J. van Koningsbruggen, *Chem. – Eur. J.*, 2019, **25**, 16766.
23 A. V. Ablov, V. I. Goldanski, K. I. Turta, R. A. Stukan, V. V. Zelentsov, E. V. Ivanov and N.V. Gerbeleu, *Dokaldy Chem.*, 1971, **196**, 1101. (Engl. Transl.)
24 S. Hayami, K. Hashiguchi, K. Inoue and Y. Maeda, *J. Nucl. Radiochem. Sci.,* 2004, **5**, N1.
25 M. A. Blagov, N. G. Spitsyna, N. S. Ovanesyan, A. S. Lobach, L. V. Zorina, S. V. Simonov, K. V. Zakharov and A. N. Vasiliev, *Dalton Trans.*, 2023, **52**, 1806.
26 B. Bleaney and D. K. Bowers, *Proc. R. Soc. London, Ser. A*, 1952, **214**, 451.
27 R. Ishikawa, T. Noda, S. Ueno, T. Okubo, H. Yamakawa, K. Sakamoto and S. Kawata, *Magnetochemistry*, 2020, **6**, 29.
28 M. S. Haddad, M. W. Lynch, W. D. Federer and D. N. Hendrickson, 1981, *Inorg. Chem.*, **20**, 1, 123.
29 M. Clemente-León, E. Coronado, M. López-Jordà, J.-F. Létard and J. Kusz, P. Gütlich, *Chem. Eur. J.*, 2010, **16**, 2207.
30 N. G. Spitsyna, M. A. Blagov, V. A. Lazarenko, R. D. Svetogorov, Y. V. Zubavichus, L. V. Zorina, O. Maximova, S. A. Yaroslavtsev, V. S. Rusakov, G. V. Raganyan, E. B. Yagubskii and A. N. Vasiliev, *Inorg. Chem.*, 2021, **60**, 23, 17462.
31 J. M. Fiddy, I. Hall, F. Grandjean, G. J. Long and U. Russo, *Journal of Physics: Condensed Matter*, 1990, **2**, 50, 10091.
32 S. Brooker, *Chem. Soc. Rev.*, 2015, **44**, 10, 2880.
33 N. Lalioti, A. Charitos, J. Parthenios, O. Malina, M. Polaskova, M. Petr and V. Tangoulis, *Molecules*, 2023, **28**, 15, 5816.
34 Q. A. Pankhurst, G. R. Thompson, V. K. Sankaranarayanan, and D. P. E. Dickson, *J. Magn. Magn. Mater.*, 1996, **155**, 104.
35 N. G. Spitsyna, M. A. Blagov, V. A. Lazarenko, L. V. Zorina, A. N. Vasiliev, V. B. Krapivin, R. D. Svetogorov, O. V. Maximova, S. V. Simonov and E. B. Yagubskii, *Dalton Trans.*, 2019,**48**, 9328.
36 J. Cirera, M. Via-Nadal, E. Ruiz, *Inorg. Chem.,* 2018, **57**, 14097.
37 D. A. Pantazis, *J. Chem. Theory Comput.*, 2019, **15**, 938.
38 L. Noodleman, *J. Chem. Phys.*, 1981, **74**, 5737.
39 M. Mitani, H. Mori, Y. Takano, D. Yamaki, Y. Yoshioka and K. Yamaguchi, *J. Chem. Phys.*, 2000, **113**, 4035.
40 S. Mandal, S. Majumder, S. Mondal and S. Mohanta, *Eur. J. Inorg. Chem.*, 2018, **41**, 4556.
41 S. Meskaldji, A. Zaiter, L. Belkhiri and A. Boucekkine, *Theor. Chem. Acc.*, 2012, **131**, 1151.

TOC

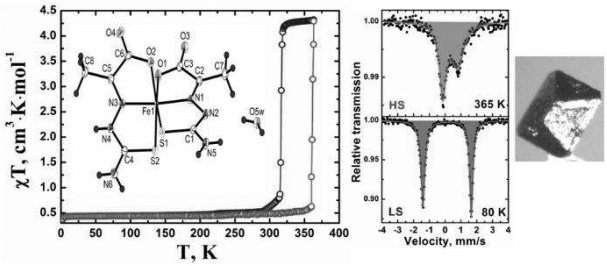

The X-ray structures and abrupt spin-crossover of the hydrate of the neutral iron(III) complex based on the pyruvic acid thiosemicarbazone ligand $[Fe^{III}(Hthpy)(thpy)]\cdot H_2O$ have been determined for the first time.